Precise and versatile microplate reader-based analyses of biosensor signals from arrayed microbial colonies

Fabian S. F. Hartmann[1, #], Tamara Weiß[1, #], Louise L. B. Kastberg[1], Christopher T. Workman[1], Gerd M. Seibold[1*]

[1]Section for Synthetic Biology, Department Bioengineering, Technical University of Denmark (DTU), Lyngby, Denmark

[#]These authors have contributed equally to this work and share first authorship

***Correspondence:** Gerd M. Seibold, Section of Synthetic Biology, Department of Biotechnology and Biomedicine, Technical University of Denmark, Søltofts Plads Building 223, DK-2800, Kongens Lyngby, Denmark; e-mail: gesei@dtu.dk

Keywords: Lab-automation, Mrx1-roGFP2, mCherry, GFP, arrayed microbial colonies, genetically encoded biosensors

Abstract

Genetically encoded fluorescent biosensors have emerged as a powerful tool to support phenotypic screenings of microbes. Optical analyses of fluorescent sensor signals from colonies grown on solid media can be challenging as imaging devices need to be equipped with appropriate filters matching the properties of fluorescent biosensors. Towards versatile fluorescence analyses of different types of biosensor signals derived from arrayed colonies, we investigate here the use of monochromator equipped microplate readers as an alternative to imaging approaches. Indeed, for analyses of the LacI-controlled expression of the reporter mCherry in *Corynebacterium glutamicum,* or promoter activity using GFP as reporter in *Saccharomyces cerevisiae*, an improved sensitivity and dynamic range was observed for a microplate reader-based analyses compared to their analyses *via* imaging. The microplate reader allowed us to capture signals of ratiometric fluorescent reporter proteins (FRPs) with a high sensitivity and thereby to further improve the analysis of internal pH via the pH-sensitive FRP mCherryEA in *Escherichia coli* colonies. Applicability of this novel technique was further demonstrated by assessing redox states in *C. glutamicum* colonies using the FRP Mrx1-roGFP2. By the use of a microplate reader, oxidative redox shifts were measured in a mutant strain lacking the non-enzymatic antioxidant mycothiol (MSH), indicating its major role for maintaining a reduced redox state also in colonies on agar plates. Taken together, analyses of biosensor signals from microbial colonies using a microplate reader allows comprehensive phenotypic screenings and thus facilitates further development of new strains for metabolic engineering and systems biology.

44 **1 Introduction**

45 Phenotypic screening of microbial strain libraries for interesting genetic variants underlies many current
46 investigations ranging from analyses of gene functions in basic research on microbial physiology to high-
47 throughput genetic engineering of tailor-made biotechnological platform organisms [1–4]. In the best case
48 scenario the trait of interest is directly coupled to a phenotypic output such as growth and/or formation
49 of a natural chromophore or fluorophore[5] allowing the easy identification of the strains of interest [6].
50 However, target phenotypes often cannot easily be detected and laborious analytical methods such as
51 HPLC-analyses of metabolite levels would be required to identify interesting candidates. In these cases,
52 genetically encoded biosensors have emerged as a valuable tool to facilitate high-throughput screenings.
53 Such biosensors provide the advantage that an intracellular signal is transduced into an output signal,
54 which can easily be measured from each strain of a library in a high-throughput manner[7,8]. Organisms
55 naturally possess a variety of different types of sensors to monitor the intra- or extracellular accumulation
56 of small molecules, ions, or changes in physical parameters. By applying synthetic biology tools, these
57 properties can be harnessed to develop biosensors for high-throughput screenings [9]. Transcription factor-
58 based biosensors (TFBs) represent some of the most common types of biosensors applied which are often
59 based on metabolite-sensing transcription factors. Upon interacting with effector molecules, the
60 expression of an actuator gene, such as a fluorescent protein, is controlled [10,11]. In contrast to TFBs,
61 fluorescent reporter proteins (FRPs) act both as sensor and actuator. FRPs can undergo conformational
62 changes upon interaction with a target metabolite or change in physiological state, which is subsequently
63 accompanied by a change in their intrinsic fluorescence characteristics [12,13]. To date, many different TFBs
64 and FRPs are available for measuring a broad range of internal metabolites or physiological states in
65 microbial cells [12–18].

66 Besides the selection of specific biosensors for the screening of strain libraries, the experimental set-up
67 also represents a major determinant to be considered for an efficient screening method. High-throughput

68 analysis of microbial libraries can be conducted in well-plates, on agar plates, via fluorescence-activated
69 cell sorting (FACS), or droplet-based screening [7]. Compared to FACS or droplet-based screening
70 approaches, screenings conducted in well-plates and on agar plates significantly lowers the throughput
71 that can be achieved. However, it provides the advantage that biosensor signals from tested strain can be
72 directly compared under various conditions [19]. Agar plate screens are considered as less laborious and
73 provide a slightly higher throughput when compared to well-plate screens. However, agar plate
74 screenings are dependent on optical readouts using camera-based imaging systems[7]. As supplier-specific
75 filters for excitation and emission are required, the flexibility for assessing different fluorescent signals is
76 low [7]. Furthermore, the fixed position of light sources and camera in the imaging system affects sensitivity
77 and might cause shadow-effects dependent of the location of the colony on the agar plate [20]. In contrast,
78 multimode plate readers equipped with monochromators and photomultipliers, commonly applied for
79 well-plate screenings, offer a high flexibility, sensitivity, and easy adaptation of reader properties to the
80 respective biosensor applied.

81 Despite the aforementioned challenges, we successfully applied the ratiometric FRP mCherryEA biosensor
82 to visualize the internal pH of *E. coli* colonies growing on agar plates measured by a FUSION FX (Vilber)
83 imaging system[8]. To adequately capture the ratiometric biosensor signals, the imaging system was
84 equipped with two capsules (excitation laser and filter module) for excitation (530 nm and 440 nm) and a
85 filter for capturing the emission (595 nm) of the pH-sensitive mCherry variant mCherryEA[8].

86 The visualization of other biosensor signals (i.e. the redox biosensor protein Mrx1-roGFP2 with an
87 excitation at 380 nm and 470 nm/ and an emission at 510 nm[16]) requires that the imaging system set-up
88 is adapted to the properties of the applied fluorescent protein. Thus, applying another fluorescent protein
89 is not readily possible if such appropriate filter modules are not available. This limitation also extends to
90 most of the widely applied imaging systems for microbial colonies, as most cannot be equipped with

91 varying and/or multiple fluorescence filter modules, and thus cannot be used to capture ratiometric
92 fluorescence signals.

93 Recently, a standard microplate reader was applied as a tool for image-based real-time gene expression
94 analysis using TFBs in living cells growing on the surface of solid media[21]. By scanning the surface of
95 rectangle OmniTray plates, fluorescence signals from organisms growing on agar allowed for imaging with
96 different resolutions (highest resolution = 360 × 240)[21]. During phenotypic screenings on agar plates,
97 strains are typically pinned from a 96-well source plate as an array of 96, 384, or 1536 colonies on
98 rectangular OmniTray plates [19]. Therefore, the positions of the arrayed colonies on the agar plates are
99 identical to the typical array of wells on conventional microplates used in microplate readers. This
100 prompted us to test standard microplate reader systems for their applicability to assess fluorescence
101 signals from arrayed colonies on agar plates.

102 In this study we demonstrate the wide applicability of microplate reader-based system to measure
103 fluorescence signals from arrayed colonies on agar plates. This method is shown for different types of
104 biosensors including a TFB based on LacI for regulated mCherry expression in *C. glutamicum*, promoter-
105 based biosensors using yeast enhanced GFP (yeGFP) as fluorescent reporter in *S. cerevisiae*, and the FRP
106 mCherryEA to assess the internal pH in *E. coli* colonies. We further show that the method developed here
107 enables the accurate measurement of redox states for *C. glutamicum* colonies via the ratiometric sensor
108 protein Mrx1-roGFP2 on agar plates.

109

110 **2 Results and Discussion**

111 **2.1 Microplate reader-based analysis of transcription factor-based biosensors in *C. glutamicum* colonies**
112 **on agar plates**

113 TFBs are widely used in microbial physiology, metabolic engineering, and synthetic biology. Many designs
114 for TFBs include fluorescent proteins as a reporter, which provides an easy optical readout to screen for
115 high or low fluorescent variants from a library. Genome wide screens are often conducted via arrayed
116 colonies on agar plates, as this approach offers a higher capacity than well-plate based screens and the
117 comparison of different conditions[7]. However, as stated above, analyses of fluorescence signals from
118 colonies via imaging can be challenging[22].

119 To compare fluorescence imaging with microplate reader-based measurements, two model strains,
120 *C. glutamicum* (pEKEx2_low-*mCherry*) and *C. glutamicum* (pEKEx2_high-*mCherry*), were constructed to
121 compare fluorescence imaging with microplate reader-based measurements. The two strains were
122 transformed using plasmids pEKEx2_low-*mCherry and* pEKEx2_high-*mCherry*, both consisting of the IPTG
123 inducible promoter P_{tac} but differed in the strength of the ribosomal binding site (RBS) for expression of
124 the reporter *mCherry* (Fig. 1a). To verify the different expression levels, C*. glutamicum* (pEKEx2_low-
125 *mCherry*) and *C. glutamicum* (pEKEx2_high-*mCherry*) were cultivated in BHI liquid medium supplemented
126 with different IPTG concentrations followed by endpoint fluorescence analysis using a microplate reader
127 (SpectraMax). As depicted in Fig. 1b, both strains revealed an IPTG dose-dependent increase of the
128 respective fluorescence intensity. As expected, the use of a stronger RBS in *C. glutamicum* (pEKEx2_high-
129 *mCherry*) resulted in a higher maximal mCherry fluorescence level when compared to C*. glutamicum*
130 (pEKEx2_low-*mCherry*). Moreover, no increased fluorescence levels were measured for the control strain
131 *C. glutamicum* (pEKEx2) with an empty vector (Fig.1b). Analysis of fluorescence levels obtained under fully
132 induced conditions (> 500 µM) revealed that fluorescence signals of all three strains were significantly

133 different to each other. In presence of the highest tested IPTG concentration (5 mM IPTG), fluorescence
134 intensities derived from the high-mCherry construct and the low-mCherry construct were approximately
135 50-fold and 5-fold higher when compared to the empty vector control, respectively (Fig. 1b). The results
136 show that the constructed TFBs possess significantly different mCherry levels and both can clearly be
137 distinguished from background fluorescence levels in liquid cultures using a microplate reader.

138

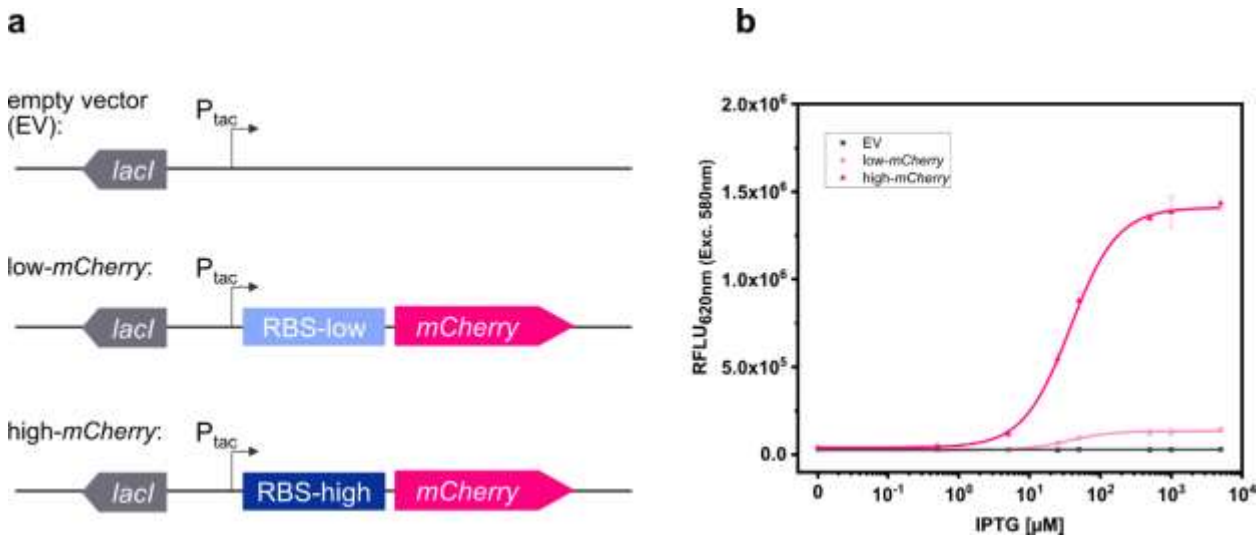

139

140 Figure 1: Schematic illustration of the genetic constructs for the expression platforms in pEKEx2 with different levels of mCherry
141 translation initiation (**a**). Relative fluorescence units [RFLU] in presence of different IPTG concentrations after over-night
142 cultivations in liquid media for *C. glutamicum* (pEKEx2) (EV: grey squares), *C. glutamicum* (pEKEx2_low_*mCherry*) (low-*mCherry*:
143 light pink circles) and *C. glutamicum* (pEKEx2_high_*mCherry*) (high-*mCherry*: dark pink triangles) (**b**). A Hill function was fit to low-
144 *mCherry* and high-*mCherry* data, and a linear fit was used for the empty vector (EV). Error bars represent standard deviation of
145 four biological replicates.

146

147 To analyze the fluorescence signals derived from colonies of the three test strains *C. glutamicum* (pEKEx2),
148 *C. glutamicum* (pEKEx2_low_*mCherry*), *and C. glutamicum* (pEKEx2_high_*mCherry*) via imaging, the
149 strains were spotted on rectangular OmniTray (Singer Instruments, United Kingdom) agar plates
150 supplemented with different IPTG concentrations (0 mM to 5mM). After 48 h of incubation, the mCherry
151 fluorescence was analyzed in a fluorescence filter equipped FUSION FX (Vilber) imaging system. In
152 presence of 5 mM IPTG, colonies carrying the reporter pEKEx2_high_*mCherry* revealed significantly higher

153 fluorescence intensities (mean value 8.10 x 10^2 ± 49 RFLU) when compared to colonies carrying the empty
154 vector control (5.11 x 10^2 ± 43 RFLU) (Figure 2a, b). In contrast, statistical analysis via ANOVA revealed
155 that fluorescence signals derived from colonies of *C. glutamicum* (*pEKEx2_low_mCherry*) (4.92 x 10^2 ±
156 24 RFLU) are not significantly different when compared to the empty vector control (Figure 2b). To note,
157 increased exposure times (increased from 800 ms to 1000 ms) resulted in higher fluorescence levels for
158 both the empty vector strain, the low-mCherry as well as high-mCherry variant (Fig. S1). Albeit,
159 fluorescence signals obtained from the high-mCherry variant reached saturation at exposure times above
160 800 ms, the signals detected for the low-mCherry variant were still indistinguishable from signals obtained
161 from the empty vector control strains under fully induced conditions (Fig. S1). Significant differences in
162 the visual detection of biosensor fluorescence are a prerequisite towards rational decision-making during
163 screens and the selection of variants. Thus, imaging is unlikely to be suitable for all biosensors and libraries
164 [7].

165 The accurate positioning of 96-arrayed colonies on rectangular agar plates (in a 96-well scheme) was used
166 to measure each colony with the optics of the plate reader. To confirm the accurate positioning of arrayed
167 colonies, we performed an absorbance scan in a 96-well scheme with 30 x 30 scans per well for an
168 OmniTray agar plate with 96- arrayed colonies in the plate reader (Fig. S2). The absorbance scan revealed
169 that each colony, corresponding to the respective well, was centered irrespectively of the position of the
170 individually measured colony (Fig. S2). The exact match of the positioning allowed the plate reader to
171 perform single point measurements similar to measurements performed using 96-well plates.
172 Accordingly, time required for analyses of the 96-colonies can be reduced from 90 minutes (scan mode)
173 to 20 seconds (endpoint mode). Thus, the signals obtained from the colonies represent an average value
174 from the colony rather than capturing heterogeneity across the colony.

175 Based on the precision and accuracy of the colony positions, the same agar plates used for fluorescence
176 imaging were now analyzed using a standard microplate reader. Fluorescence analysis revealed that

177 signals detected via the plate reader for colonies equipped with the high-mCherry construct (average
178 fluorescence of $1.98 \times 10^5 \pm 5.01 \times 10^3$ RFLU), as well as for colonies with the low-mCherry construct
179 ($2.13 \times 10^4 \pm 7.34 \times 10^2$ RFLU), were significantly different when compared to the empty vector control
180 ($4.96 \times 10^3 \pm 2.88 \times 10^2$ RFLU) (Fig. 2c).

181 In addition, we tested the dose-dependent response of the TFB carrying strains
182 *C. glutamicum* (pEKEx2_low_mCherry and *C. glutamicum* (pEKEx2_high_mCherry) on agar plates with a
183 series of different IPTG concentrations (0 to 5 mM IPTG; Fig. 2d). Hereby, similar dose-response curves
184 were obtained for all strains when compared to the liquid cultures (Fig. 1b). As expected, no IPTG
185 dependent increase of mCherry fluorescence was detected for colonies of the empty vector control strain
186 *C. glutamicum* (pEKEx2). These results demonstrate that a microplate reader can be used for assessing
187 fluorescence signals in arrayed colonies.

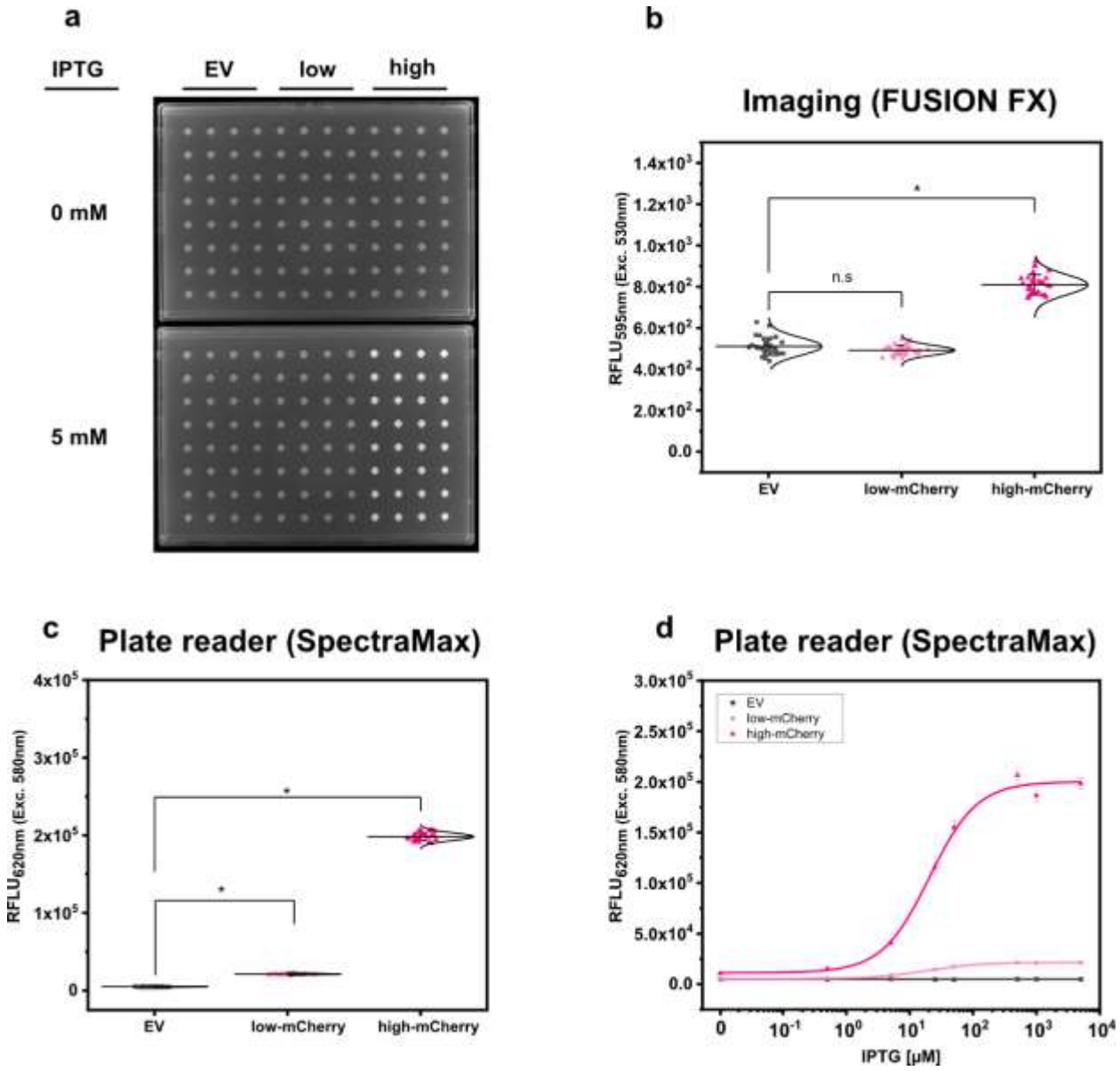

Figure 2: Comparison of fluorescence detection of arrayed bacterial colonies on agar plates via imaging and plate reader-based analysis. Representative fluorescence image of 32 colonies of *C. glutamicum* WT (pEKEx2) (EV: grey squares), *C. glutamicum* WT (pEKEx2_*low_mCherry*) (low: light pink circles) and *C. glutamicum* WT (pEKEx2_high_*mCherry*) (high: dark pink triangles) are spotted in absence (0 mM) or presence (5 mM) of IPTG by the use of the imaging system FUSION FX (Vilber) (**a**), the respective relative fluorescence units [RFLU] of determined for the different colonies (**b**) and the RFLU values of *C. glutamicum* colonies recorded via a plate reader (SpectraMax iD3 multi-mode plate reader (Molecular Devices LLC, U.S.A)) (**c**). RFLU values determined for arrayed colonies of *C. glutamicum* (pEKEx2) (EV: grey squares), *C. glutamicum* (pEKEx2_low_*mCherry*) (low-*mCherry*: light pink circles) and *C. glutamicum* (pEKEx2_high_*mCherry*) (high-*mCherry*: dark pink triangles) cultivated in presence of different IPTG concentrations (**d**). For sigmoidal curve fitting, Hill's equation (low-mCherry and high-mCherry). For the empty vector (EV), a linear fit was used. For fluorescence analysis using the plate reader excitation and emission were set to 580 nm and 620 nm, respectively. Imaging of arrayed colonies on agar plates was conducted using the imaging system FUSION FX (Vilber) equipped with a capsule for excitation (530 nm) and an emission filter (595 nm). Fluorescence signals were statistically analyzed with one-way-ANOVA followed by Tukey´s test ($^{n.s}$ $p > 0.05$; * $p \leq 0.001$). Error bars represent standard deviation of 32 colonies.

204 **2.2 Microplate reader-based system for improved fluorescence analysis of promoter-based biosensors**
205 **in *Saccharomyces cerevisiae* colonies on agar plates**

206 We next addressed the applicability of the microplate reader-based method for the analysis of
207 fluorescence signals from the broadly used fluorescent protein GFP in colonies of the well-known model-
208 organism S. *cerevisiae.* For this purpose, two model strains of the haploid prototrophic yeast *S. cerevisiae*
209 CEN.PK113-7D[23] were constructed by integration of expression cassettes with yeGFP as optical readout.
210 Towards the development of reporter systems with different expression levels, a well-characterized weak
211 constitutive promoter (PDA1) and strong glycolytic promoter (TDH3) were used to control varying levels
212 of yeGFP production [24]. Prior to analyzing the fluorescence signals from *S. cerevisiae* (background control),
213 *S. cerevisiae* (PDA1-yeGFP) (weak promoter), and *S. cerevisiae* (TDH3p-yeGFP) (strong promoter), strains
214 were arrayed on OmniTray agar plates.

215 First, fluorescence analyses of GFP signals from arrayed *S. cerevisiae* colonies was performed using the
216 microbial colony CCD imaging workstation Phenobooth (Singer Instruments), equipped with the
217 manufacturer's filters for GFP fluorescence. As depicted in Fig. 3a, all colonies of *S. cerevisiae*
218 (background) and *S. cerevisiae* (PDA1-yeGFP) (weak promoter) revealed fluorescence intensities at the
219 same level. In contrast, significantly increased mean fluorescence intensities (1.28 ± 0.14 fold) were
220 measured for colonies of *S. cerevisiae* (TDH3p-yeGFP) (strong promoter). However, individual signals from
221 colonies equipped with the strong promoter still partly overlap with the values derived from the
222 background control colonies. This means that during a random screen a high number of "GFP positive"
223 strains would have remained undetected resulting in a low screening efficiency. Next, fluorescence signals
224 were analyzed by the use of the imaging system FUSION FX (Vilber), equipped with a capsule and a filter
225 for excitation at 435nm and emission at 480nm, respectively. The mean fluorescence signals derived from
226 96 colonies of *S. cerevisiae* (PDA1-yeGFP) (weak promoter) and *S. cerevisiae* (TDH3p-yeGFP) (strong
227 promoter) were significantly increased by 1.30 ± 0.10 fold and 2.37 ± 0.22 fold when compared to the

228 background control, respectively (Fig. 3b). Even though not all individual colonies of *S. cerevisiae* (PDA1-
229 yeGFP) can explicitly be distinguished from colonies of the control *S. cerevisiae* strain, which shows
230 background levels of fluorescence, fluorescence analysis via the FUSION FX imaging system has
231 significantly been improved when compared to the use of an imaging workstation (Phenobooth, Singer
232 Instruments).

233 As a next step, the microplate reader-based method was used to analyze yeGFP signals derived from the
234 different promoters in *S. cerevisiae*. As described for mCherry signals in *C. glutamicum* by the use of the
235 microplate reader SpectraMax, an average value of $6.62 \times 10^4 \pm 8.59 \times 10^3$ RFLU, $1.19 \times 10^5 \pm 1.22 \times 10^4$
236 RFLU and $7.46 \times 10^5 \pm 8.74 \times 10^4$ RFLU was determined for *S. cerevisiae* (background), *S. cerevisiae* (PDA1-
237 yeGFP) (weak promoter) and *S. cerevisiae* (TDH3p-yeGFP) (strong promoter), respectively (Fig. 3c). This
238 corresponds to a significant 1.80 ± 0.16 fold (weak promoter) and 11.30 ± 1.02 fold (strong promoter)
239 increase when compared to the background control. In contrast to fluorescence imaging, all individual
240 signals obtained for the 96 analyzed colonies harboring both the weak promoter (PDA1-yeGFP) or the
241 strong promoter (TDH3p-yeGFP) possessed higher fluorescence levels when compared to background
242 control colonies (Fig. 3c).

243 To demonstrate transferability of the microplate reader-based approach, we next analyzed fluorescence
244 signals in arrayed colonies using a CLARIOstar^{Plus} as a different plate reader device. When compared to
245 *S. cerevisiae*, the mean fluorescence intensity measured for all colonies equipped with the weak promoter
246 (PDA1-yeGFP) and strong promoter (TDH3p-yeGFP) were increased 1.93 ± 0.13 fold and 12.36 ± 0.89 fold,
247 respectively (Fig. 3d). These results are in accordance with results obtained via the SpectraMax plate
248 reader.

249 Taken together, microplate reader-based analysis of colony fluorescence enables the precise and sensitive
250 detection of fluorescence levels of reporter proteins in various microorganisms. To facilitate fluorescence

analysis via this approach it is required that the colonies are arrayed in a microtiter-based format. If it is not possible to array the microbial colonies, fluorescence analysis via sensitive imaging systems equipped with adequate sets of filters, such as those used here for the FUSION FX (Vilber) imaging system, are a good alternative, although their incorporation in highly automated workflows is a challenge.

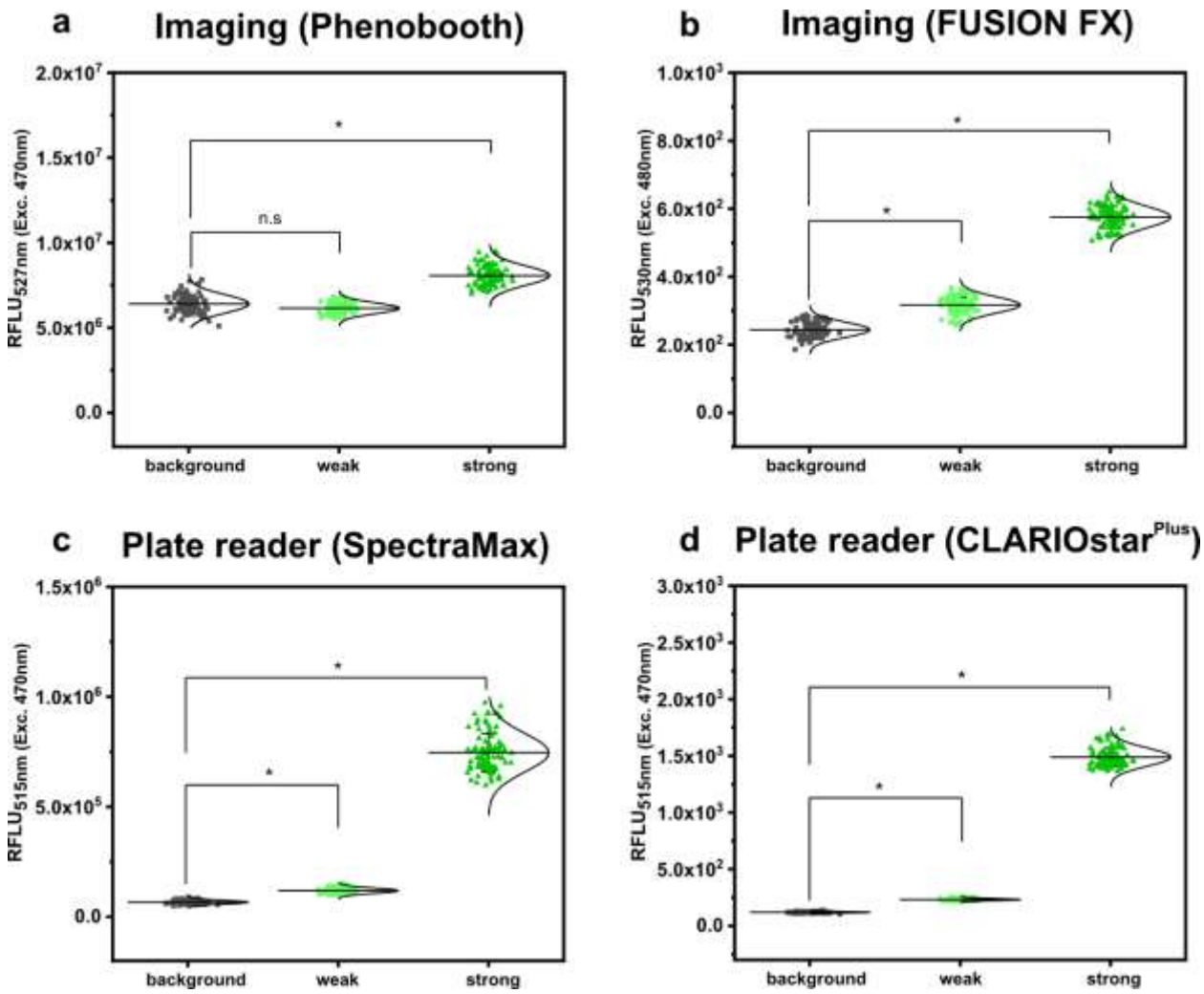

Figure 3: Comparison of fluorescence detection of arrayed *Saccharomyces cerevisiae* colonies on agar plates via imaging and plate reader-based analysis. Relative fluorescence units (RFLU) of 96-arrayed colonies of *Saccharomyces cerevisiae* (background; grey squares), *Saccharomyces cerevisiae* (TDH3p-yeGFP) (weak; light green circles) and *Saccharomyces cerevisiae* (PDA1p-yeGFP) (strong, green triangles) analyzed via imaging using the Phenobooth (**a**) or the FUSION FX (Vilber) (**b**). Further, fluorescence analysis was performed using the plate reader devices SpectraMax (**c**) and CLARIOstar^{Plus} (**d**). RFLU were obtained by normalizing the fluorescence intensity to the colony size (perimeter). Fluorescence signals were statistically analyzed with one-way-ANOVA followed by Tukey´s test ($^{n.s}$ $p > 0.05$; * $p \leq 0.001$). Mean values from 96- replicates are shown (solid horizontal line).

264 **2.3 Microplate reader-based analysis of the pH-sensitive protein mCherryEA improves accuracy of**
265 **internal pH measurements in *E. coli* colonies**

266 The use of a monochromator equipped microplate reader allowed us to set optimal excitation and
267 emission wavelength settings for the sensitive detection of mCherry and GFP signals from microbial
268 colonies. To test if the versatility and precision of the wavelength settings via the monochromators also
269 enables sensitive analyses of fluorescence signals from ratiometric fluorescent reporter proteins, we
270 aimed to compare analysis of fluorescence signals from the internal pH-sensor protein mCherryEA in
271 arrayed *E. coli* colonies via a plate reader to the recently described approach via fluorescence imaging in
272 a FUSION FX (Vilber) imaging system[8].

273 For this purpose, colonies of the strain *E. coli* MG1655 (pXMJ19_*mCherryEA*) and the empty vector control
274 strain *E. coli* MG1655 (pXMJ19) were arrayed on SB agar plates (pH 7.0). After cultivation, 5 µL of PBS
275 buffer supplemented with 0.05 % CTAB and with set pH values between 7.0 and 8.5 were applied onto
276 the colonies, as recently described [8]. At this CTAB concentration the *E. coli* cell membrane is permeabilized
277 allowing the internal pH to become adjusted to the set external pH [17]. The fluorescence of the colonies
278 was analyzed using an excitation scan (400 nm – 590 nm) at an emission wavelength of 630 nm and using
279 the positions of the 96-well measurement mode of the plate reader. As depicted in Fig. 4a, two excitation
280 maxima at 454 nm and 580 nm were obtained for colonies of *E. coli* MG1655 (pXMJ19_*mCherryEA*), which
281 are in accordance to the maxima observed in recently performed excitation scans of bacterial strains
282 harboring the pH- sensitive mCherryEA protein in liquid culture[8,25]. As expected, no characteristic
283 mCherryEA sensor signal was measured for the empty vector control *E. coli* MG1655 (pXMJ19) (Fig. 4a).
284 When applying PBS buffer (+ CTAB) with a set pH of 7.0 to the colonies, an emission intensity of
285 5.8E + 06 FLU was measured at 454 nm excitation, whereas the signal obtained upon an excitation at
286 580 nm was higher with 6.8E + 06 FLU (Fig. 4a); when a PBS buffer (+ CTAB) with a higher pH (8.5) was
287 applied to a colony, the fluorescence intensity obtained for an excitation at 454 nm increased (8.3E + 06

288 FLU) and decreased at an excitation at 580 nm (4.4E + 06 FLU). This pH-dependent response of the signals
289 for mCherryEA at the two excitation wavelengths indicates that the ratiometric response of the biosensor
290 protein mCherryEA in *E. coli* colonies on agar plates can be measured using the microplate reader-based
291 system. Further, fluorescence from *E. coli* MG1655 (pXMJ19_*mCherryEA*) colonies treated with PBS buffer
292 (+ CTAB) with set pH values ranging from 7.0 to 8.5 (Fig. 4b) were analyzed using the plate reader (Exc.
293 454 nm/ 580 nm) and the recently established imaging method (Exc. 440 nm/ Exc. 530 nm) [8]. The
294 biosensor ratios determined for the imaging method increased linear from 0.62 ± 0.02 (pH 7.0) to 1.08 ±
295 0.03 (pH 8.5) upon increasing the pH (Fig. 4b). A similar biosensor response was detected with the
296 microplate reader-based method, resulting in an increase from 0.85 ± 0.03 (pH 7.0) to 1.35 ± 0.03 (pH 8.5)
297 (Fig. 4b).

298 Next, 120 colonies arrayed on a rectangular agar plate were analyzed *via* the two different methods
299 (imaging and plate reader) and the internal pH for each colony determined and visualized with a heat
300 map, where each square corresponds to a single colony (Fig. 4c). For both methods, the mean internal pH
301 obtained by the imaging method and the plate reader method was similar with 7.66 ± 0.13 and 7.65 ± 0.03,
302 respectively (Fig. 4d). This agrees with the reported cytoplasmic pH of *E. coli* which is normally maintained
303 within the range of 7.4-7.9[26–28] and recently determined internal pH levels in *E. coli* MG1655 colonies on
304 agar plates under similar conditions[8]. However, differences with respect to the distribution of the
305 determined internal pH values were observed when comparing the data obtained for the two different
306 methods (Fig. 4d). The plate reader method established here allowed us to narrow down the distribution
307 from 7.26-7.82 (ΔpH= 0.56; imaging method) to 7.59-7.76 (ΔpH= 0.17; plate reader method),
308 corresponding to a reduction of 0.39 pH units. As the pH is logarithmically and inversely related to the
309 concentrations of hydrogen ions in a solution, the accuracy of the analysis is improved by 390 %. The
310 broader distribution obtained by the imaging method might be caused by reflection artefacts from the
311 transparent edges of the OmniTray plates. To note, the imaging method relies on a one-step excitation of

312 the whole plate, whereas measurements performed in the microplate reader allowed us to measure
313 colonies individually, similar to measurements performed in a 96-well microplate. Moreover, the
314 microplate reader-based method allows operators to set excitation and emission wavelengths on demand
315 and thus perfectly matches the two excitation maxima displayed by the sensor protein mCherryEA. In
316 contrast, the imaging system FUSION FX (Vilber) needs to be equipped with the most suited capsules and
317 filters available (Exc. 440 nm & Exc. 530 nm), which often do not match the properties of the fluorescent
318 protein[25,29,30].

319

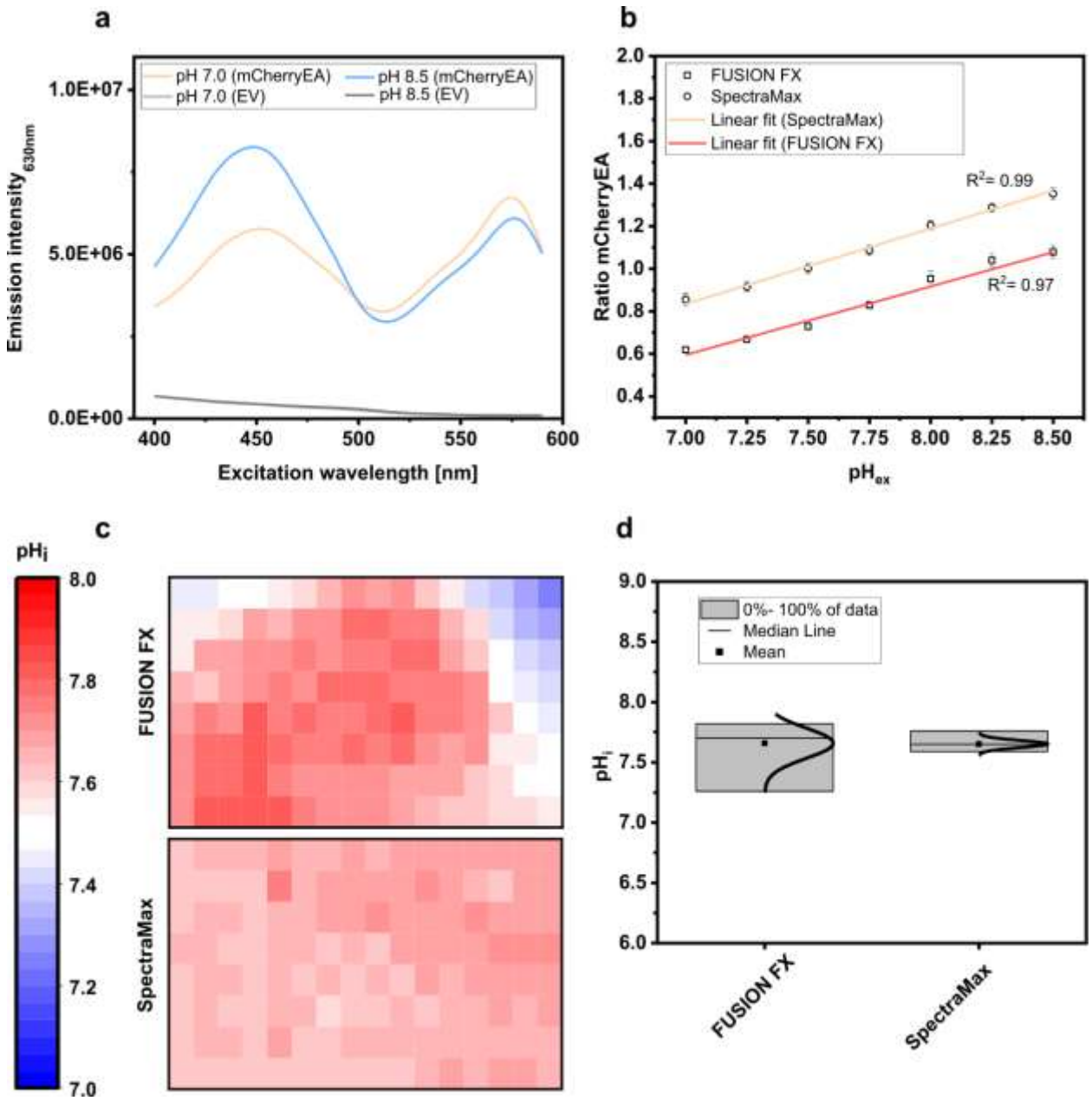

Figure 4: Excitation scan (400 nm – 590 nm) recording the emission intensity at 630 nm in colonies of *E. coli* MG1655 (pXMJ19_*mCherryEA*) (mCherryEA) and the empty vector control strain *E. coli* MG1655 (pXMJ19) (EV) after applying 5 µL PBS buffer supplemented with cetyltrimethylammonium bromide (CTAB; final concentration 0.05 % (w/v)) with a set pH of 7.0 and 8.5 (**a**) and ratiometric biosensor signals obtained by dividing the emission intensity at 454 nm by 580 nm upon applying PBS buffer with pH values ranging from 7.0 – 8.5 (**b**). Calculation of the internal pH for biosensor signals recorded from 120 colonies either *via* imaging using the FUSION FX imaging system equipped with two capsules (Exc. 440 nm & Exc. 530 nm) and one emission filter (Em. 595 nm) as recently described in Hartmann et al. 2022[8] or with a microplate reader system (SpectraMax) (**c**) and data distribution with median and mean values obtained by the two different approaches (**d**). Error bars represent standard deviation from at least three replicates.

332 **2.4 Mycothiol is required to maintain a reduced environment in *C. glutamicum* colonies growing on agar**
333 **plates**

334 The improved accuracy using the plate reader-based biosensor analysis represents a significant step
335 forward with respect to screening approaches requiring high sensitivities. Moreover, the high flexibility
336 brought by the monochromatic technology of the plate reader device easily adapts to other fluorescent
337 reporter proteins without causing additional costs and effort to equip imaging devices with appropriate
338 filters. Thus, we next tested this novel technique by applying a ratiometric redox biosensor protein called
339 Mrx1-roGFP2 in *C. glutamicum* colonies.

340 The abundant low molecular weight (LMW) mycothiol (MSH) functions to maintain the reduced state of
341 the cytoplasm and represents the main non-enzymatic antioxidant in high-GC Gram-positive bacteria,
342 such as the industrial amino acid producer *C. glutamicum* [31–33]. Recently, the genetically encoded redox
343 biosensor protein Mrx1-roGFP2 was successfully applied in *C. glutamicum* WT and the MSH-deficient
344 mutant strain *C. glutamicum* Δ*mshC* to monitor dynamic redox changes in liquid cultures[16,34]. Mutant
345 strains lacking MSH have revealed high susceptibility towards oxidative stress resulting in an impaired
346 growth behavior when cells were exposed to artificial oxidants in shaker-flasks[32]. In absence of artificial
347 oxidants, growth of the MSH-deficient mutant strain proceeded similar to the wild type strain[16,32,34], even
348 though biosensor measurements in the mutant strain revealed an oxidative redox shift [16,34]. Detecting
349 intracellular changes (i.e. oxidative stress) prior to the occurrence of a growth defect is an important
350 advance for the development of highly sensitive sensor-based screening approaches. This prompted us to
351 test the analysis of intracellular redox states in arrayed colonies of *C. glutamicum* WT and a mutant strain
352 lacking MSH using the redox biosensor protein Mrx1-roGFP2.

353 To analyze the redox states in *C. glutamicum* colonies, the 380 nm/470 nm biosensor ratios from 120
354 arrayed colonies of WT_Mrx1- roGFP2 and the MSH-deficient mutant strain Δ*mshC*_Mrx1-roGFP2 were

355 determined. The Mrx1-roGFP2 biosensor consists of redox sensitive GFP2 (roGFP2) which harbors two Cys
356 residues. Upon oxidation it forms a disulfide bond, resulting in an increase of the respective biosensor
357 ratio (Exc. 380 nm/ Exc. 470 nm), whereas it responds in the opposite way upon reduction of the
358 biosensor protein. As depicted in Fig. 5a, the mean values of the biosensor ratios were significantly
359 different with 0.82 ± 0.01 and 1.52 ± 0.02 for WT_Mrx1-roGFP2 and Δ*mshC*_Mrx1-roGFP2, respectively,
360 indicating a more oxidized state of the biosensor protein Mrx1-roGFP2 in the Δ*mshC*_Mrx1-roGFP2 strain
361 background on agar plates (Fig. 5a). This is in accordance to previous measurements conducted in liquid
362 cultures with biosensor ratios of 1.0 ± 0.02 (WT_Mrx1-roGFP2) and 1.52 ± 0.03 (Δ*mshC*_Mrx1-roGFP2)[16].

363 Further, we validated the dynamic response and functionality of the sensor protein Mrx1-roGFP2 in
364 colonies by applying Dithiothreitol (DTT; 100 mM) and Natriumhypochlorite (NaOCl; 100 mM) as reducing
365 and oxidizing agents, respectively. For this, 5 µL drops were applied onto WT_Mrx1-roGFP2 and
366 Δ*mshC*_Mrx1-roGFP2 colonies followed by real-time monitoring of the biosensor signals. Prior to the
367 colony treatment, WT_Mrx1-roGFP2 was maintaining stable biosensor ratios between 0.76 - 0.78
368 followed by a strong reduction or increase of the biosensor ratio upon applying DTT or NaOCl, respectively
369 (Fig. 5b). After five minutes of incubation, fully reduced (DTT; biosensor ratio of 0.53) and fully oxidized
370 (NaOCl; biosensor ratio of 1.4) biosensor ratios were recorded until the end of the experiment (Fig. 5b).
371 The treatment with PBS only temporarily induced a slight decrease of the recorded biosensor ratio but
372 then was restored to initially recorded biosensor ratios (Fig. 5b). In contrast, Δ*mshC*_Mrx1-roGFP2
373 colonies revealed biosensor ratios between 1.4 - 1.45 prior to the treatment of the colonies. The addition
374 of DTT buffer solution resulted in a strong reduction of the biosensor ratio reaching fully reduced ratios
375 of 0.54, six to eight minutes following the treatment (Fig. 5c). As expected, treatment with NaOCl just
376 slightly increased the ratio to 1.54 due to its almost fully oxidized state, when compared to a final
377 biosensor ratio of 1.4 for colonies treated with PBS buffer only (Fig. 5c). To note, no alteration of the
378 recorded fluorescence signals was observed when performing the same experiment using the

379 *C. glutamicum* WT controls strain, indicating that the measured change of the ratiometric biosensor
380 signals in both sensor strains can be attributed to the biosensor protein Mrx1-roGFP2 (Fig. S3).

381 Based on the measured biosensor ratios, the oxidation degree (OxD) of the biosensor protein Mrx1-
382 roGFP2 was calculated according to equation 1. OxD values of 0.93 ± 0.03 and 0.33 ± 0.03 were calculated
383 for the Mrx1-roGFP2 biosensor in Δ*mshC*_Mrx1-roGFP2 and WT_Mrx1-roGFP2 colonies on agar plates,
384 respectively (Fig. 5d). The results are consistent with previous studies performed in shaker-flasks under
385 non-stressed conditions where OxD values between 0.3 - 0.5 were reported for WT_Mrx1- roGFP2[16,34]. In
386 contrast, almost fully oxidized biosensor states were reported for the MSH-deficient mutant strain (OxD
387 = 0.8 - 0.95)[16,34]. Upon the formation of ROS, the redox-active sulfhydryl group of MSH can either scavenge
388 free radicals directly or functions as a cofactor for antioxidant enzymes resulting in formation of oxidized
389 mycothiol disulfide (MSSM)[31,35–38]. Accordingly, the lack of MSH elevates the intracellular ROS levels and
390 in turn induces an auto-oxidation of the biosensor protein Mrx1- roGFP2 in Δ*mshC*_Mrx1-roGFP2. Thus,
391 previous results and the results of this study indicate the major role of MSH for the overall redox
392 homeostasis under aerobic growth conditions in shake-flasks cultivations but also in colonies growing on
393 agar plates.

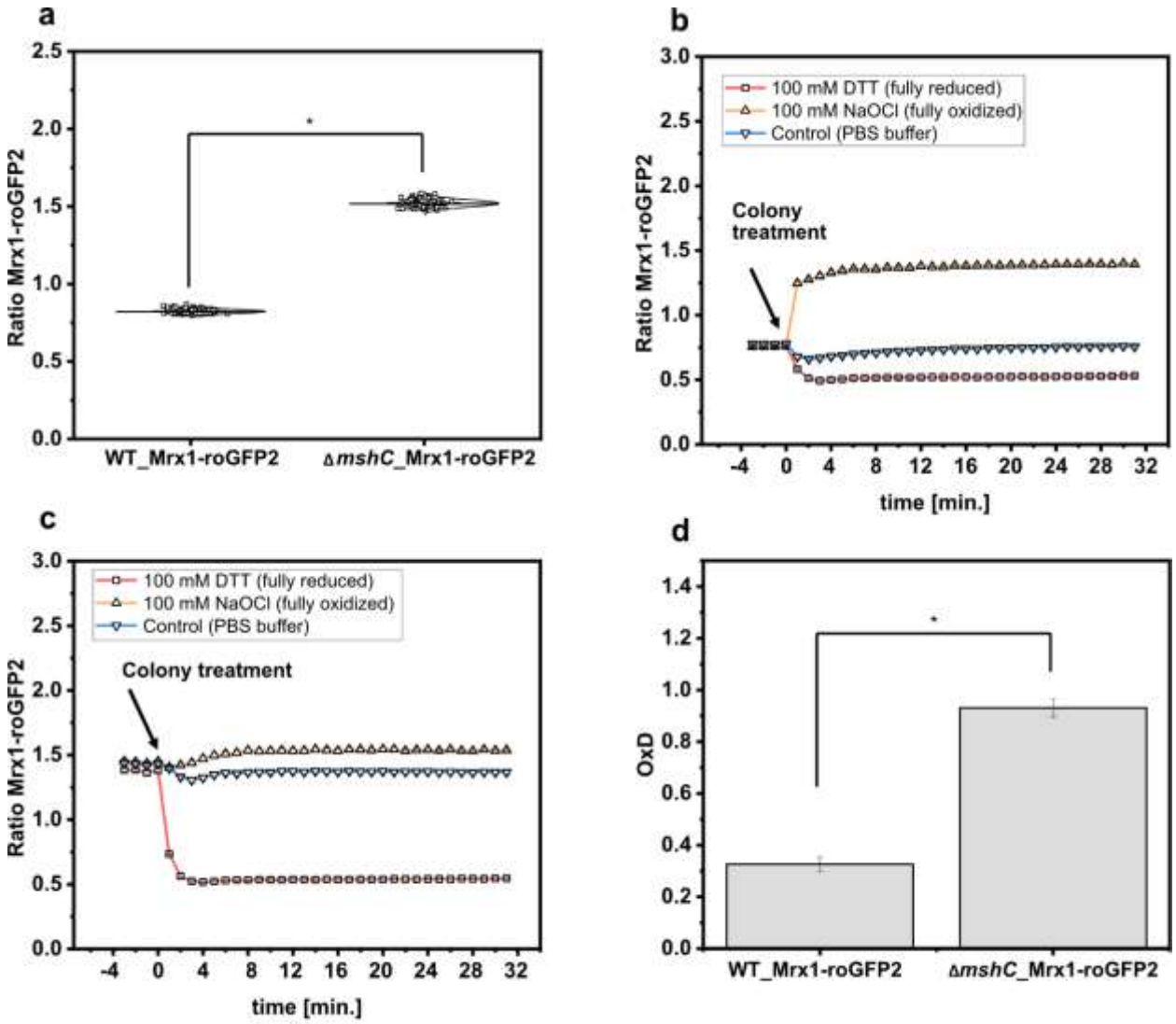

Figure 5: Calculated biosensor ratio (Exc. 380nm/ Exc. 470 nm) of the sensor protein Mrx1-roGFP2 in colonies of *C. glutamicum* WT_Mrx1-roGFP2 (WT_Mrx1-roGFP2) and *C. glutamicum* Δ*mshC*_Mrx1-roGFP2 (Δ*mshC*_Mrx1-roGFP2) (**a**) and real-time monitoring of the response of the ratiometric signal of the biosensor Mrx1-roGFP2 upon applying DTT (100 mM) (reducing agent), hypochlorite (100 mM) (oxidizing agent) and PBS buffer (control) onto WT_Mrx1-roGFP2 (**b**) and Δ*mshC*_Mrx1-roGFP2 colonies (**c**). Calculation of the oxidation degree (OxD) by normalizing biosensor ratios to fully oxidized and reduced states (**d**). For sensor analysis, 30 colonies from four independent agar plates and experiments were analyzed for each strain (120 colonies in total). Biosensor ratios were analyzed with one-way-ANOVA followed by Tukey´s test ($^{n.s}$ $p > 0.05$; * $p \leq 0.001$).

407 **2.5 Ratiometric biosensor signals are independent of the colony size**

408 Fluorescence signals derived from single fluorescent proteins need to be normalized to the OD_{600} (96-well
409 screen) or colony size (agar screen). In contrast to single fluorescent proteins, a ratiometric fluorescent
410 protein can be normalized to the second fluorescence signal rather than growth related parameters. This
411 implies that a ratiometric biosensor signal should not be affected by changes of the colony size during
412 screens on agar plates.

413 To test this, a dilution series (different set OD_{600}) of *C. glutamicum* WT (WT), *C. glutamicum* WT_Mrx1-
414 roGFP2 (WT_Mrx1-roGFP2) and *C. glutamicum* Δ*mshC*_Mrx1-roGFP2 (Δ*mshC*_Mrx1-roGFP2) was spotted
415 on rectangular OmniTray plates with solidified CGXII minimal medium (1 % Glucose) (Fig. 6a). After 48
416 hours of incubation, the final colony size was determined for all spotted dilutions and the size reduction
417 calculated relative to the highest applied OD_{600} (Fig. 6a). For the highest applied OD_{600} (10^1), defined as
418 100 % colony size, the area was determined to be 680 ± 29, 610 ± 52 and 590 ± 49 pixels for the WT,
419 WT_Mrx1-roGFP2 and the Δ*mshC*_Mrx1-roGFP2 colonies, respectively (Fig. 6a). Upon applying higher
420 dilutions (stepwise 1:10), the relative colony size was reduced by approximately 10 % for each dilution
421 step and a relative colony size of 55 ± 8 %, 61 ± 2% and 54 ± 0.4 % was reached upon applying an OD_{600} of
422 10^{-3} for the WT, WT_Mrx1-roGFP2 and Δ*mshC*_Mrx1-roGFP2 strain, respectively (Fig. 6a). For this dilution,
423 the circular morphology of the colonies was impaired leading to inaccuracies with respect to the colony
424 size determination for further dilutions (Fig. 6a). Next, the positions of the arrayed colonies from the
425 dilution series were selected and the fluorescence intensity derived from the sensor protein Mrx1-roGFP2
426 analyzed. Absolute fluorescence intensities measured at 510 nm (Exc. 470 nm) revealed increased
427 fluorescence levels in colonies of WT_Mrx1-roGFP2 (5.4×10^6 – 1.3×10^7 FLU) and Δ*mshC*_Mrx1-roGFP2
428 (4.2×10^6 – 1.03×10^7 FLU) strains when compared to the parental wild type strain *C. glutamicum* (1.90 –
429 3.90×10^6 FLU) (Fig. 6b). Absolute fluorescence intensities decreased upon a reduction of the colony size
430 (Fig. 6b). In accordance with the fluorescence analysis for mCherry or GFP in the previous sections, relative

431 fluorescence intensities were calculated by normalizing the absolute fluorescence intensity to the
432 perimeter of the colony. As expected, fluorescence signals normalized to the measured perimeter of the
433 colonies resulted in stable relative fluorescence intensities until a colony size reduction of 70 % was
434 reached (Fig. S4). Next, the second fluorescence signal (Exc. 380 nm/Em. 510 nm) was measured for all
435 colonies and the biosensor ratio calculated (Exc. 380 nm/ Exc. 470 nm). The ratiometric biosensor signal
436 independently of the colony size, remained stable between 1.0 – 1.1 and 1.4 – 1.5 in WT_Mrx1-roGFP2
437 and Δ*mshC*_Mrx1-roGFP2 colonies, respectively (Fig. 6c). As discussed in the previous section, higher
438 biosensor ratios measured for the MSH-deficient strain are caused by the more oxidized state of the
439 biosensor protein Mrx1-roGFP in this strain background. To note, increased ratiometric signals (between
440 2.5 to 4.0) for the agar surface (no colony) and for *C. glutamicum* not harboring the biosensor protein
441 Mrx1-roGFP2 are due to low background fluorescence at 510 nm (Exc. 470 nm) but a higher background
442 fluorescence at 510 nm when excited at 380 nm (Fig. 6c).

443 Taken together, the results demonstrate that the signal derived from a ratiometric biosensor is robust
444 against variations of colony size and the morphology of colonies (Fig. 6c). This makes ratiometric FRPs a
445 powerful tool when conducting screens of mutant libraries comprising different phenotypes (e.g. growth
446 behavior). Furthermore, agar plate-based screens provide the advantage that the tested strains can be
447 exposed to various conditions at the same time (replica plating) [19,39]. Conducting screens under industrially
448 relevant conditions (e.g. pH gradients) supported by the use of ratiometric "stress" biosensors will
449 facilitate the development of structured metabolic models for industrially relevant organisms. This bridges
450 metabolic engineering and bioprocess development allowing for the development of computational
451 models suitable for both cell factory design and process optimization at industrial scales in the future [40].

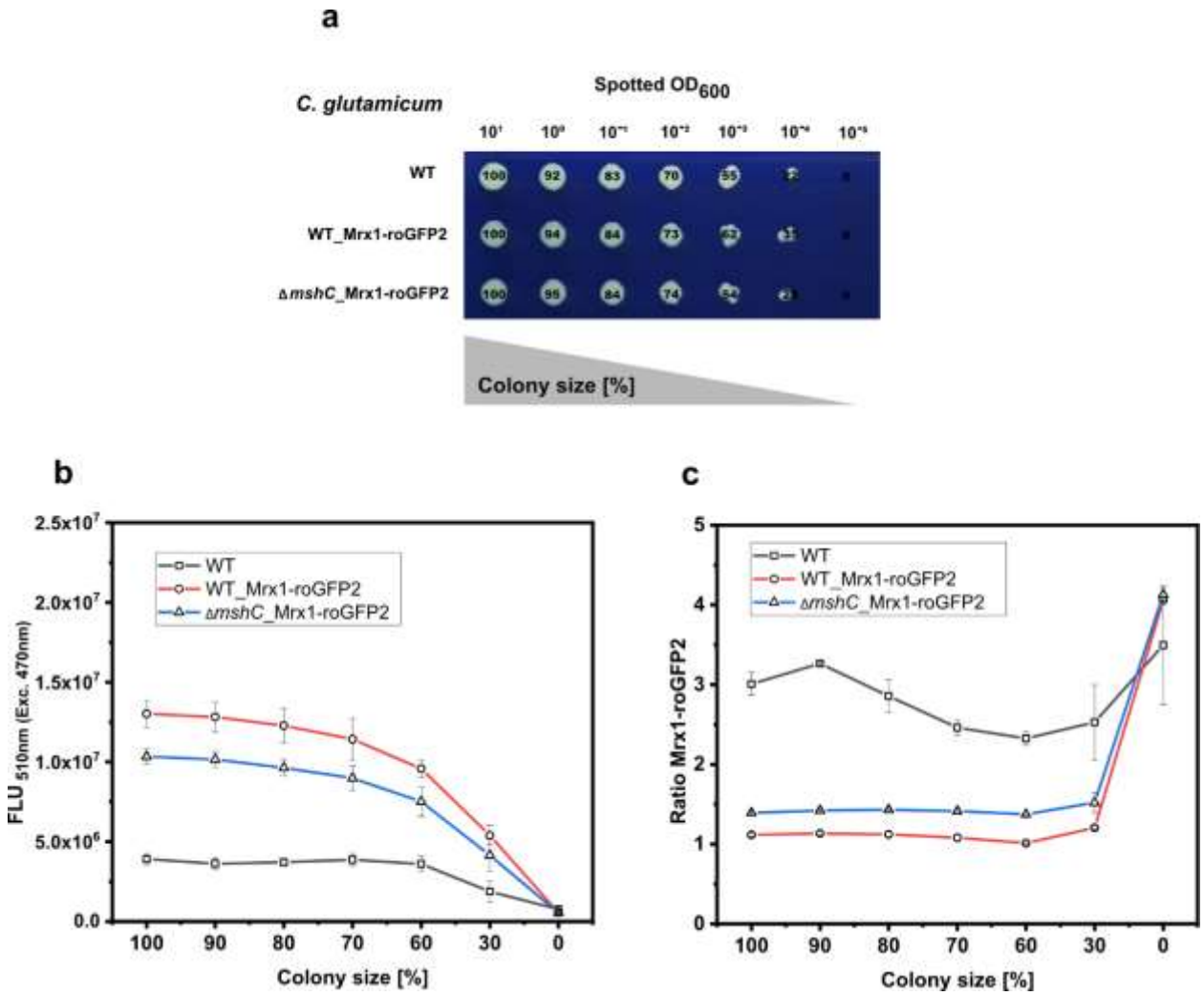

Figure 6: Robotic spotting of a dilution series of *C. glutamicum* WT (WT), *C. glutamicum* WT_Mrx1-roGFP2 (WT_Mrx1-roGFP2) and *C. glutamicum* Δ*mshC*_Mrx1-roGFP2 (Δ*mshC*_Mrx1-roGFP2) liquid cultures with different set optical densities measured at 600 nm (OD_{600}) and determination of the colony size relative to the highest spotted OD_{600} (**a**). Absolute fluorescence intensities measured at 510 nm (Exc. 470 nm) to validate the presence of Mrx1- roGFP2 in WT_Mrx1-roGFP2 and Δ*mshC*_Mrx1-roGFP2 colonies (**b**), and the ratiometric biosensor signal of Mrx1-roGFP2 in the different colonies (**c**). Robotic spotting was performed using a replica plating Robot ROTOR. Dilution series was grown on OmniTray plates with CGXII media supplemented with 1% Glucose. Fluorescence analysis of the colonies from the dilution series was performed in a microplate reader (SpectraMax iD3). For the calculation of the ratiometric biosensor signal, the emission intensity at 510 nm was recorded upon an excitation at 380 nm and 470 nm and the former was divided by the latter (Exc. 380 nm/ Exc. 470 nm). Mean values from two independent experiments are shown.

467 **3 Conclusion**

468 Phenotypic screenings using arrayed colonies is a widely applied approach to screen strain libraries for
469 particular variants with desired phenotypes. Genetically encoded biosensors are powerful analytical tools
470 to support the rational decision making for strain selection as intracellular states can easily be assessed in
471 a high-throughput manner. However, imaging analysis often limits the applicability of biosensors as the
472 optical set-up of the utilized imaging device does not match with the properties of the fluorescent protein.
473 The microplate reader-based system for sensor analysis established here provides the advantage of a
474 monochromatic technology, which provides high flexibility with respect to different excitation and
475 emission wavelengths. This novel technique has revealed high sensitivity for the detection of low
476 fluorescence levels making it attractive for the development and optimization of genetic circuits
477 regulating harmful targets. In addition, the monochromatic technology enables great opportunities to
478 utilize FRPs, which application to date is often limited due to their complex ratiometric fluorescent
479 properties. The ratiometric readout makes these types of biosensors highly robust against signal
480 fluctuations caused by the colony size or morphology of the colony. Moreover, applications of such
481 biosensors enables the measurement of complex intracellular states such as oxidative stress or the
482 internal pH in real- time due to their fast dynamics. The microplate reader-based analysis established here
483 can easily be adapted to further biosensors and combinations thereof without causing additional costs
484 and effort to install adequate filter modules. Thus, this technique is expected to provide new possibilities
485 for comprehensive phenotypic screenings and novel applications in metabolic engineering and systems
486 biology.

487

488 **4 Materials and methods**

489 **Strains, media, and culture conditions**

490 Bacterial strains, yeast strains, and plasmids used in this study are listed in Table 1. Cloning was carried
491 out using *E. coli* DH5 α, cultivated in Lysogeny Broth (LB) medium[41]. *C. glutamicum* was cultivated using
492 BHI- media (Sigma Aldrich, Germany). *E. coli* MG1655 was cultivated in SB- medium (5 g/L yeast extract;
493 10 g/L BactoTryptone; 100 mM NaCL; 50 mM KCl, buffered with 50 mM TRIS; pH 7.0) as recently
494 described[8]. For preparation of agar plates, 16 g/L agar was added to the respective media. Strains carrying
495 plasmids were cultivated in presence of kanamycin (50 µg/mL) or chloramphenicol (20 µg/mL). If required
496 and unless stated otherwise, 1 mM IPTG was added to induce gene expression. The haploid prototrophic
497 yeast *Saccharomyces cerevisiae* strain CEN.PK113-7D was grown in standard yeast peptone dextrose (YPD)
498 medium containing 10 g/L yeast extract, 20 g/L peptone, and 20 g/L glucose and incubated at 30°C. For
499 preparation of YPD agar plates 20 g/L agar was added. For selection of yeast with antibiotic resistance
500 marker NatMX, medium was supplemented with 100mg/L nourseothricin (ClonNat, Jena Bioscience).

501

502 *Table 1: Bacterial strains, yeast strains and plasmids used in this study.*

Bacterial Strains/ Plasmids	**Description**	**Reference/ Resource**
Escherichia coli		
E. coli DH5 α	F-ϕ80dlacZ Δ(lacZYA-argF) U169 deoRsupE44ΔlacU169 (f80lacZDM15) hsdR17 recA1 endA1 (rk- mk+) supE44gyrA96 thi-1 gyrA69 relA1	42
E. coli MG 1655	F^- lambda- ilvG-rfb-50rpH-1	43
E. coli MG 1655 (pXMJ19)	*E. coli* MG 1655 carrying the vector pXMJ19	8
E. coli MG1655 (pXMJ19_*mCherryEA*)	*E. coli* MG 1655 carrying a derivative of pXMJ19 for IPTG-inducible *mCherryEA* expression	8
Corynebacterium glutamicum **ATCC 13032**	**Wild type**	44

C. glutamicum (pEKEx2)	*C. glutamicum* WT carrying the shuttle vector pEKEx2	This study
C. glutamicum (pEKEx2_low_*mCherry*)	*C. glutamicum* WT carrying a derivative of the shuttle vector pEKEx2 for IPTG inducible expression of the *mCherry* gene	This study
C. glutamicum (pEKEx2_high_*mCherry*)	*C. glutamicum* WT carrying a derivative of the shuttle vector pEKEx2 for IPTG inducible expression of the *mCherry* gene	This study
C. glutamicum WT_Mrx1-roGFP2	*C. glutamicum* WT with integrated P_{tuf}-*mrx1-roGFP2* into the intergenic region of *cg1121-cg1122*	[34]
C. glutamicum Δ*mshC* _Mrx1-roGFP2	*C. glutamicum* WT deletion of *mshC* and integrated P_{tuf}-*mrx1-roGFP2* into the intergenic region of *cg1121-cg1122*	[34]
S. cerevisiae **CEN.PK113-7D**	**Wild type**	[23]
*S. cerevisiae (*TDH3p-yeGFP_XII-1)	*S. cerevisiae with integrated TDH3p-yeGFP-CYC1t and NatMX resistance cassette into the intergenic integration site XII-1*	This study
*S. cerevisiae (*PDA1p-yeGFP_XII-1)	*S. cerevisiae with integrated PDA1p-yeGFP-CYC1t and NatMX resistance cassette into the intergenic integration site XII-1*	This study
Plasmids		
pEKEx2	Expression vector; p*tac lacI*^{q} Km^r	[45]
pXMJ19	Expression vector; p*tac lacI*^{q} Cam^r	[46]
pEKEx2_low_*mCherry*	pEKEx2 derivative for IPTG-inducible *mCherry* gene expression. Upstream of *mCherry* a weak RBS was inserted.	This study
pEKEx2_high_*mCherry*	pEKEx2 derivative for IPTG-inducible *mCherry* gene expression. Upstream of *mCherry* a high RBS including a spacer of 6 nt was inserted. This RBS-spacer combination was reported as strong RBS by Shi et al. 2018.[47]	This study
pXMJ19_*mCherryEA*	pXMJ19 derivative for IPTG-inducible *mCherryEA* gene expression	[8]
pCfB2197	EasyClone system-based yeast integrative vector carrying loxP-flanked natMX marker, integration into	[48]

	S. cerevisiae XII-1 chromosomal location, USER site for cloning amp resistance.	
pLK0106	pCfB2197 containing yeGFP gene under control of PDA1 promoter.	This study
pLK0107	pCfB2197 containing yeGFP gene under control of TDH3 promoter.	This study

503

504

505 **Strain construction**

506 The two plasmids pEKEx2_low_*mCherry* and pEKEx2_high_*mCherry* were assembled *via* Gibson cloning
507 using the Gibson Assembly® Master Mix (NEB, USA) according to the manufacturer's instructions. For his
508 purpose pEKEx2 was first linearized using SacI (NEB, USA). The gene for mCherry was amplified by PCR
509 using the primer pairs low_*mCherry*_fw and low_mCherry_rev (Table S1) or high_*mCherry*_fw and
510 high_*mCherry*_rev for pEKEx2_low_*mCherry* and pEKEx2_high_*mCherry*, respectively. All plasmids were
511 introduced into competent *E. coli* DH5α and analyzed via sequencing prior to further use. Transformation
512 of electrocompetent *C. glutamicum* cells and strain validation were performed as described previously[49].

513 To construct the two plasmids pLK0106 and pLK0107 for yeast, DNA fragments constituting the weak
514 PDA1 promoter or the strong TDH3 promoter [24] and the yeGFP open reading frame [50] were synthesized
515 as double-stranded gene fragments (Twist Bioscience). The integrative vector pCfB2197 from the
516 EasyClone 2.0 toolkit was used for plasmid construction, which allowed for selection in prototrophic
517 strains [48]. Briefly, the vector was linearized by digestion with *AsiSI* (Life Technologies) restriction
518 endonuclease and nicked with *Nb.BsmI* (New England BioLabs). Synthetic DNA fragments were PCR-
519 amplified - using forward primer FW_USER_TDH3 or FW_USER_PDA1 combined with reverse primer
520 RV_USER_yeGFP - and subsequently cloned into the linearized vector backbone by uracil-excision based
521 (USER) cloning technique [51,52]. Plasmids were transformed into *E. coli* for storage and amplification.
522 Correct plasmid assembly was verified by PCR and Sanger sequencing (Eurofins Genomics) using primers

523 ADH1_test_fw and CYC1_test_rv. Constructed integrative vectors (pLK0106 and pLK0107) were *NotI* (Life
524 Technologies) digested to capture the linear fragments for integration. *S. cerevisiae* was transformed as
525 previously described [53]. For genetic integration of cassettes, 1 µg of linear DNA was transformed into yeast
526 for integration into the XII-1 chromosomal integration site [54]. Cells were plated onto selective YPD plates
527 and colonies were re-streaked on selective plates. Genomic DNA was extracted as previously described [55],
528 and integration verified by PCR using XII-1_up and XII-1_down. All oligonucleotides used in this study can
529 be found in the supplementary material (Table S1).

530

531 **Fluorescence analysis**

532 Fluorescence measurements of liquid cultures were conducted in black clear-bottomed 96-well
533 microplates (Greiner Bio-One, Austria) using a SpectraMax iD3 multi-mode plate reader (Molecular
534 Devices LLC, U.S.A). For fluorescence analysis of the fluorescent protein mCherry, endpoint measurements
535 were recorded by setting the excitation wavelength at 580 nm and the emission wavelength at 620 nm.
536 For liquid cultures, fluorescence intensities were normalized to the optical density measured at 600 nm
537 (OD_{600}) using transparent flat-bottomed 96-well microplates (Greiner bio-one B.V., Netherlands). Prior to
538 measurements of liquid cultures, cells were washed and four times concentrated.

539 For fluorescence analysis of the pH-sensitive protein mCherryEA, excitation scans were recorded by
540 setting the excitation wavelength between 400 nm and 590 nm and the emission wavelength at 630 nm.
541 For ratiometric analysis of the biosensor signal, the emission maxima obtained upon an excitation at
542 454 nm and 580 nm were taken and the corresponding biosensor ratio was calculated by dividing the
543 former emission intensity by the latter as recently described[8]. For fluorescence analysis of the redox
544 biosensor protein Mrx1-roGFP2, the calculation of Exc. 380 nm/ Exc. 470 nm (Em. 510 nm) was used for
545 the determination of the biosensor ratio as recently described[16]. For determination of the biosensor

546 oxidation degree (OxD), biosensor ratios from untreated samples were normalized to fully reduced
547 (100 mM Dithiothreitol (DTT) in PBS buffer; pH 7.0) or oxidized (100 mM Natriumhypochlorite (NaOCl) in
548 PBS buffer, pH 7.0) samples according to equation1. Here, $I380_{sample}$ and $I470_{sample}$ represent the measured
549 fluorescence intensities received for an excitation at 380 nm and 470 nm, respectively. Fully reduced and
550 oxidized controls are given by $I380_{red}$, $I470_{red}$ and $I380_{ox}$, $I470_{ox}$, respectively.

$$OxD = \frac{I380_{sample}\ x\ I470_{red} - I380_{red}\ x\ I470_{sample}}{I380_{sample}\ x\ I470_{red} - I380_{sample}\ x\ I470_{ox} + I380_{ox}\ x\ I470_{sample} - I380_{red}\ x\ I470_{sample}} \quad (1)$$

551

552

553 **Microplate reader-based analysis of sensor signals in colonies on agar plates**

554 Prior to robotic spotting of cell cultures, wells of 96-well microtiter plates (Greiner bio-one B.V.,
555 Netherlands) were filled with 200 µL overnight culture adjusted to an OD_{600} of 1 in the respective media.
556 For dilution series, the OD_{600} was set to 10 and 1:10 dilutions prepared in microtiter plates. The working
557 plate (96-well plate) was used as a source plate for robotic spotting using a ROTOR HDA benchtop robot
558 (Singer Instruments, United Kingdom) on rectangular OmniTray plates (Singer Instruments, United
559 Kingdom) with solidified medium on the target plate as recently described[8]. The OmniTray plates were
560 prepared by using 50 mL of the respective media supplemented with appropriate antibiotic and IPTG for
561 biosensor expression if required. Agar plates with spotted cell cultures in an arrayed format were
562 cultivated for 24 hours (*E. coli* and *S. cerevisiae* strains) or 48 hours for *C. glutamicum* strains if not
563 otherwise stated. Fluorescence analysis was performed using a SpectraMax iD3 multi-mode plate reader
564 (Molecular Devices LLC, U.S.A). Prior to fluorescence analysis, the lid from the OmniTray plate was
565 removed. A 96-well plate scheme was selected for the measurement mode and the wells selected for

566 targeting the respective colonies arrayed in a 96-well scheme on the agar plates. Measurement height
567 was set to 5 mm and measurements were performed at ambient temperature.

568

569 **Fluorescence imaging of arrayed colonies**

570 Fluorescence imaging of microbial colonies on agar plates was carried out using the photo-documentation
571 system FUSION FX (Vilber Lourmat, France) and the FUSION FX EVOLUTION-CAPT software (Vilber
572 Lourmat) for image analyses. For fluorescence analysis of the fluorescent protein mCherry, the FUSION FX
573 was equipped with a capsule for excitation at 530 nm and an emission filter at 595 nm. For yeGFP analysis
574 a capsule for excitation at 480 nm and a filter for emission 530 nm were used. Exposure time was set to
575 800 msec if not stated otherwise. Biosensor signals from the pH- sensitive protein mCherryEA were
576 measured using the FUSION FX as recently described [8]. For fluorescence analysis using the Phenobooth
577 (Singer Instruments, United Kingdom), the blue channel was selected for excitation (470 nm) and the
578 emission intensity measured using a GFP filter (527 nm/ 20 nm).

579

580 **White light imaging and determination of colony sizes**

581 White light images were captured using the Phenobooth (Singer Instruments, United Kingdom). If
582 required, images were processed prior to analyzing the images using Cellprofiler 4 (version 4.0.7) [56]. In
583 order to determine colony sizes, the respective images were analyzed *via* the Python toolbox Pyphe [57].

584

585 **Statistical analysis**

586 Biosensor signals were analyzed using one-way variance (ANOVA) followed by Tukey´s test. The respective
587 analysis was performed using Python 3 [58], and Pandas [59] was used to handle data frames. ANOVA was

performed using the ols() and anova_lm() function of the statsmodels package [60]. Tukey´s test was performed using tukey_hsd() function of the bioinfokit package [61]. Differences were considered significant when p-value < 0.05. All data were plotted and visualized using the software Origin.

Abbreviations

CTAB	Cetyltrimethylammonium bromide
DTT	Dithiothreitol
EV	Empty vector
FRP	Fluorescent reporter protein
GFP	Green fluorescent protein
IPTG	Isopropyl β- d-1-thiogalactopyranoside
OD	Optical density
OxD	Oxidation degree
RBS	Ribosomal binding site
RFLU	Relative fluorescence units
roGFP2	Redox sensitive GFP2
TFB	Transcription factor-based biosensor
WT	Wild type

Credit author statement

Fabian S. F. Hartmann: Conceptualization; Data curation, Formal analysis, Investigation, Methodology, Validation, Visualization, Writing of original draft; Writing-review & editing; **Tamara Weiß:** Conceptualization; Data curation, Formal analysis, Investigation, Methodology, Validation, Visualization, Writing of original draft; Writing-review & editing; **Louise L. B. Kastberg:** Formal analysis, Investigation, Writing-review & editing; **Christopher T. Workman:** Funding acquisition, Writing-review & editing; **Gerd M. Seibold:** Conceptualization; Funding acquisition; Supervision; Writing-original draft; Writing-review & editing.

Funding

605 This work received funding by the Novo Nordisk Fonden within the framework of the Fermentation-based
606 Biomanufacturing Initiative (FBM) (FBM-grant: NNF17SA0031362) and from the Bio Based Industries Joint
607 Undertaking under the European Union´s Horizon 2020 research and innovation program (Grant
608 agreement No 790507).

609

610 **Availability of data and materials**

611 All data generated and analyzed during this study are included in this article and its additional files. Raw
612 datasets are available from the corresponding author on reasonable request.

613

614 **Conflict of Interest**

615 The authors declare that the research was conducted in the absence of any commercial or financial
616 relationships that could be construed as a potential conflict of interest.

617

618 **Acknowledgment**

619 We would like to thank the Fermentation Core at DTU Bioengineering for excellent technical support.

620

621 **References**

622 (1) French, S.; Coutts, B. E.; Brown, E. D. Open-Source High-Throughput Phenomics of Bacterial
623 Promoter-Reporter Strains. *Cell Syst.* **2018**, *7* (3), 339-346.e3.
624 https://doi.org/10.1016/j.cels.2018.07.004.

625 (2) Nichols, R. J.; Sen, S.; Choo, Y. J.; Beltrao, P.; Zietek, M.; Chaba, R.; Lee, S.; Kazmierczak, K. M.;
626 Lee, K. J.; Wong, A.; Shales, M.; Lovett, S.; Winkler, M. E.; Krogan, N. J.; Typas, A.; Gross, C. A.
627 Phenotypic Landscape of a Bacterial Cell. *Cell* **2011**, *144* (1), 143–156.
628 https://doi.org/10.1016/j.cell.2010.11.052.

629 (3) Liu, W.; Jiang, R. Combinatorial and High-Throughput Screening Approaches for Strain
630 Engineering. *Appl. Microbiol. Biotechnol.* **2015**, *99* (5), 2093–2104.
631 https://doi.org/10.1007/s00253-015-6400-0.

632 (4) Zeng, W.; Guo, L.; Xu, S.; Chen, J.; Zhou, J. High-Throughput Screening Technology in Industrial
633 Biotechnology. *Trends Biotechnol.* **2020**, *38* (8), 888–906.

634 https://doi.org/10.1016/j.tibtech.2020.01.001.

635 (5) Tanaka, Y.; Sasaki, N.; Ohmiya, A. Biosynthesis of Plant Pigments: Anthocyanins, Betalains and
636 Carotenoids. *Plant J.* **2008**, *54* (4), 733–749. https://doi.org/10.1111/j.1365-313X.2008.03447.x.

637 (6) Peters, J. M.; Colavin, A.; Shi, H.; Czarny, T. L.; Larson, M. H.; Wong, S.; Hawkins, J. S.; Lu, C. H. S.;
638 Koo, B. M.; Marta, E.; Shiver, A. L.; Whitehead, E. H.; Weissman, J. S.; Brown, E. D.; Qi, L. S.;
639 Huang, K. C.; Gross, C. A. A Comprehensive, CRISPR-Based Functional Analysis of Essential Genes
640 in Bacteria. *Cell* **2016**, *165* (6), 1493–1506. https://doi.org/10.1016/j.cell.2016.05.003.

641 (7) Kaczmarek, J. A.; Prather, K. L. J. Effective Use of Biosensors for High-Throughput Library
642 Screening for Metabolite Production. *J. Ind. Microbiol. Biotechnol.* **2021**, *48* (9–10).
643 https://doi.org/10.1093/jimb/kuab049.

644 (8) Hartmann, F. S. F.; Weiß, T.; Shen, J.; Smahajcsik, D.; Savickas, S.; Seibold, G. M. Visualizing the pH
645 in *Escherichia coli* Colonies via the Sensor Protein mCherryEA Allows High-Throughput Screening
646 of Mutant Libraries. *mSystems* **2022**, 2021.07.08.451719.
647 https://doi.org/doi.org/10.1128/msystems.00219-22.

648 (9) Schallmey, M.; Frunzke, J.; Eggeling, L.; Marienhagen, J. Looking for the Pick of the Bunch: High-
649 Throughput Screening of Producing Microorganisms with Biosensors. *Curr. Opin. Biotechnol.*
650 **2014**, *26*, 148–154. https://doi.org/10.1016/j.copbio.2014.01.005.

651 (10) Ding, N.; Zhou, S.; Deng, Y. Transcription-Factor-Based Biosensor Engineering for Applications in
652 Synthetic Biology. *ACS Synth. Biol.* **2021**, *10* (5). https://doi.org/10.1021/acssynbio.0c00252.

653 (11) Mahr, R.; Frunzke, J. Transcription Factor-Based Biosensors in Biotechnology: Current State and
654 Future Prospects. *Appl. Microbiol. Biotechnol.* **2016**, *100* (1), 79–90.
655 https://doi.org/10.1007/s00253-015-7090-3.

656 (12) Bermejo, C.; Haerizadeh, F.; Takanaga, H.; Chermak, D.; Frommer, W. B. Optical Sensors for
657 Measuring Dynamic Changes of Cytosolic Metabolite Levels in Yeast. *Nat. Protoc.* **2011**, *6* (11),
658 1806–1817. https://doi.org/10.1038/nprot.2011.391.

659 (13) Martynov, V. I.; Pakhomov, A. A.; Deyev, I. E.; Petrenko, A. G. Genetically Encoded Fluorescent
660 Indicators for Live Cell pH Imaging. *Biochim. Biophys. Acta - Gen. Subj.* **2018**, *1862* (12), 2924–
661 2939. https://doi.org/10.1016/j.bbagen.2018.09.013.

662 (14) Martinez, K. A.; Kitko, R. D.; Mershon, J. P.; Adcox, H. E.; Malek, K. A.; Berkmen, M. B.;
663 Slonczewski, J. L. Cytoplasmic pH Response to Acid Stress in Individual Cells of *Escherichia coli* and
664 *Bacillus subtilis* Observed by Fluorescence Ratio Imaging Microscopy. *Appl. Environ. Microbiol.*
665 **2012**, *78* (10), 3706–3714. https://doi.org/10.1128/AEM.00354-12.

666 (15) Depaoli, M. R.; Bischof, H.; Eroglu, E.; Burgstaller, S.; Ramadani-Muja, J.; Rauter, T.; Schinagl, M.;
667 Waldeck-Weiermair, M.; Hay, J. C.; Graier, W. F.; Malli, R. Live Cell Imaging of Signaling and
668 Metabolic Activities. *Pharmacol. Ther.* **2019**, *202*, 98–119.
669 https://doi.org/10.1016/j.pharmthera.2019.06.003.

670 (16) Hartmann, F. S. F.; Clermont, L.; Tung, Q. N.; Antelmann, H.; Seibold, G. M. The Industrial
671 Organism *Corynebacterium glutamicum* Requires Mycothiol as Antioxidant to Resist against
672 Oxidative Stress in Bioreactor Cultivations. *Antioxidants* **2020**, *9* (10), 1–13.
673 https://doi.org/10.3390/antiox9100969.

674 (17) Goldbeck, O.; Eck, A. W.; Seibold, G. M. Real Time Monitoring of NADPH Concentrations in
675 *Corynebacterium glutamicum* and *Escherichia coli* via the Genetically Encoded Sensor mBFP.
676 *Front. Microbiol.* **2018**, *9* (OCT), 1–10. https://doi.org/10.3389/fmicb.2018.02564.

677 (18) Hartmann, F. S. F.; Anastasiou, I.; Weiß, T.; Lkhaasuren, T. Combined Sensor-Based Monitoring of
678 Mycothiol Redox Potential and DNA-Damage Response in *Corynebacterium glutamicum*. *bioRxiv*
679 **2022**. https://doi.org/https://doi.org/10.1101/2022.07.25.501298.

680 (19) Aguiar-Cervera, J. E.; Delneri, D.; Severn, O. A High-throughput Screening Method for the
681 Discovery of Saccharomyces and Non- Saccharomyces Yeasts with Potential in the Brewing
682 Industry . *Eng. Biol.* **2021**, *5* (3), 72–80. https://doi.org/10.1049/enb2.12013.

683 (20) Daniel, B.; Lawless, C. Modelling Competition for Nutrients between Microbial Populations
684 Growing on a Solid Agar Surface. *bioRxiv* **2017**. https://doi.org/10.1101/086835.

685 (21) Hennessy, R. C.; Stougaard, P.; Olsson, S. A Microplate Reader-Based System for Visualizing
686 Transcriptional Activity during in Vivo Microbial Interactions in Space and Time. *Sci. Rep.* **2017**, *7*
687 (1). https://doi.org/10.1038/s41598-017-00296-4.

688 (22) Göttert, H.; Mattiazzi Usaj, M.; Rosebrock, A. P.; Andrews, B. J. Reporter-Based Synthetic Genetic
689 Array Analysis: A Functional Genomics Approach for Investigating Transcript or Protein
690 Abundance Using Fluorescent Proteins in *Saccharomyces cerevisiae*. In *Methods in Molecular*
691 *Biology*; 2018; Vol. 1672. https://doi.org/10.1007/978-1-4939-7306-4_40.

692 (23) Entian, K. D.; Kötter, P. 25 Yeast Genetic Strain and Plasmid Collections. *Methods Microbiol.* **2007**,
693 *36* (06), 629–666. https://doi.org/10.1016/S0580-9517(06)36025-4.

694 (24) Peng, B.; Williams, T. C.; Henry, M.; Nielsen, L. K.; Vickers, C. E. Controlling Heterologous Gene
695 Expression in Yeast Cell Factories on Different Carbon Substrates and across the Diauxic Shift: A
696 Comparison of Yeast Promoter Activities. *Microb. Cell Fact.* **2015**, *14* (1), 1–11.
697 https://doi.org/10.1186/s12934-015-0278-5.

698 (25) Rajendran, M.; Claywell, B.; Haynes, E. P.; Scales, U.; Henning, C. K.; Tantama, M. Imaging pH
699 Dynamics Simultaneously in Two Cellular Compartments Using a Ratiometric pH-Sensitive
700 Mutant of mCherry. *ACS Omega* **2018**, *3* (8). https://doi.org/10.1021/acsomega.8b00655.

701 (26) Wilks, J. C.; Slonczewski, J. L. pH of the Cytoplasm and Periplasm of *Escherichia coli*: Rapid
702 Measurement by Green Fluorescent Protein Fluorimetry. *J. Bacteriol.* **2007**, *189* (15), 5601–5607.
703 https://doi.org/10.1128/JB.00615-07.

704 (27) Salmond, C. V.; Kroll, R. G.; Booth, I. R. The Effect of Food Preservatives on pH Homeostasis in
705 *Escherichia coli*. *J. Gen. Microbiol.* **1984**, *130* (11), 2845–2850.
706 https://doi.org/10.1099/00221287-130-11-2845.

707 (28) Padan, E.; Zilberstein, D.; Schuldiner, S. pH Homeostasis in Bacteria. *BBA - Rev. Biomembr.* **1981**,
708 *650* (2–3), 151–166. https://doi.org/10.1016/0304-4157(81)90004-6.

709 (29) Piatkevich, K. D.; Malashkevich, V. N.; Almo, S. C.; Verkhusha, V. V. Engineering ESPT Pathways
710 Based on Structural Analysis of LSSmKate Red Fluorescent Proteins with Large Stokes Shift. *J. Am.*
711 *Chem. Soc.* **2010**, *132* (31), 10762–10770. https://doi.org/10.1021/ja101974k.

712 (30) Hartmann, F. S. F.; Anastasiou, I.; Weiß, T.; Shen, J.; Seibold, G. M. Impedance Flow Cytometry for
713 Viability Analysis of *Corynebacterium glutamicum*. *J. Microbiol. Methods* **2021**, *191* (September),

714 106347. https://doi.org/10.1016/j.mimet.2021.106347.

715 (31) Reyes, A. M.; Pedre, B.; De Armas, M. I.; Tossounian, M. A.; Radi, R.; Messens, J.; Trujillo, M.
716 Chemistry and Redox Biology of Mycothiol. *Antioxidants Redox Signal.* **2018**, *28* (6), 487–504.
717 https://doi.org/10.1089/ars.2017.7074.

718 (32) Chi, B. K.; Busche, T.; Van Laer, K.; Bäsell, K.; Becher, D.; Clermont, L.; Seibold, G. M.; Persicke, M.;
719 Kalinowski, J.; Messens, J.; Antelmann, H. Protein S-Mycothiolation Functions as Redox-Switch
720 and Thiol Protection Mechanism in *Corynebacterium glutamicum* under Hypochlorite Stress.
721 *Antioxidants Redox Signal.* **2014**, *20* (4), 589–605. https://doi.org/10.1089/ars.2013.5423.

722 (33) Liu, Y. B.; Long, M. X.; Yin, Y. J.; Si, M. R.; Zhang, L.; Lu, Z. Q.; Wang, Y.; Shen, X. H. Physiological
723 Roles of Mycothiol in Detoxification and Tolerance to Multiple Poisonous Chemicals in
724 *Corynebacterium glutamicum*. *Arch. Microbiol.* **2013**, *195* (6), 419–429.
725 https://doi.org/10.1007/s00203-013-0889-3.

726 (34) Tung, Q. N.; Loi, V. Van; Busche, T.; Nerlich, A.; Mieth, M.; Milse, J.; Kalinowski, J.; Hocke, A. C.;
727 Antelmann, H. Stable Integration of the Mrx1-roGFP2 Biosensor to Monitor Dynamic Changes of
728 the Mycothiol Redox Potential in *Corynebacterium glutamicum*. *Redox Biol.* **2019**, *20*, 514–525.
729 https://doi.org/10.1016/j.redox.2018.11.012.

730 (35) Si, M.; Xu, Y.; Wang, T.; Long, M.; Ding, W.; Chen, C.; Guan, X.; Liu, Y.; Wang, Y.; Shen, X.; Liu, S. J.
731 Functional Characterization of a Mycothiol Peroxidase in *Corynebacterium glutamicum* That Uses
732 Both Mycoredoxin and Thioredoxin Reducing Systems in the Response to Oxidative Stress.
733 *Biochem. J.* **2015**, *469* (1), 45–57. https://doi.org/10.1042/BJ20141080.

734 (36) Pedre, B.; Van Molle, I.; Villadangos, A. F.; Wahni, K.; Vertommen, D.; Turell, L.; Erdogan, H.;
735 Mateos, L. M.; Messens, J. The *Corynebacterium glutamicum* Mycothiol Peroxidase Is a Reactive
736 Oxygen Species-Scavenging Enzyme That Shows Promiscuity in Thiol Redox Control. *Mol.*
737 *Microbiol.* **2015**, *96* (6), 1176–1191. https://doi.org/10.1111/mmi.12998.

738 (37) Tossounian, M. A.; Pedre, B.; Wahni, K.; Erdogan, H.; Vertommen, D.; Van Molle, I.; Messens, J.
739 *Corynebacterium diphtheriae* Methionine Sulfoxide Reductase a Exploits a Unique Mycothiol
740 Redox Relay Mechanism. *J. Biol. Chem.* **2015**, *290* (18), 11365–11375.
741 https://doi.org/10.1074/jbc.M114.632596.

742 (38) Si, M.; Zhao, C.; Zhang, B.; Wei, D.; Chen, K.; Yang, X.; Xiao, H.; Shen, X. Overexpression of
743 Mycothiol Disulfide Reductase Enhances *Corynebacterium glutamicum* Robustness by
744 Modulating Cellular Redox Homeostasis and Antioxidant Proteins under Oxidative Stress. *Sci.*
745 *Rep.* **2016**, *6* (July), 1–14. https://doi.org/10.1038/srep29491.

746 (39) Navarrete, C.; Estrada, M.; Martínez, J. L. *Debaryomyces hansenii*: An Old Acquaintance for a
747 Fresh Start in the Era of the Green Biotechnology. *World J. Microbiol. Biotechnol.* **2022**, *38* (6), 1–
748 10. https://doi.org/10.1007/s11274-022-03280-x.

749 (40) Hartmann, F. S. F.; Udugama, I. A.; Seibold, G. M.; Sugiyama, H.; Gernaey, K. V. Digital Models in
750 Biotechnology : Towards Multi-Scale Integration and Implementation. *Biotechnol. Adv.* **2022**, *60*,
751 108015. https://doi.org/10.1016/j.biotechadv.2022.108015.

752 (41) Bertani, G. Lysogeny at Mid-Twentieth Century: P1, P2, and Other Experimental Systems. *J.*
753 *Bacteriol.* **2004**, *186* (3), 595–600. https://doi.org/10.1128/JB.186.3.595-600.2004.

754 (42) Studier, F. W.; Moffatt, B. A. Use of Bacteriophage T7 RNA Polymerase to Direct Selective High-

755 Level Expression of Cloned Genes. *J. Mol. Biol.* **1986**, *189* (1), 113–130.
756 https://doi.org/10.1016/0022-2836(86)90385-2.

757 (43) Blattner, F. R.; Plunkett, G.; Bloch, C. A.; Perna, N. T.; Burland, V.; Riley, M.; Collado-Vides, J.;
758 Glasner, J. D.; Rode, C. K.; Mayhew, G. F.; Gregor, J.; Davis, N. W.; Kirkpatrick, H. A.; Goeden, M.
759 A.; Rose, D. J.; Mau, B.; Shao, Y. The Complete Genome Sequence of *Escherichia coli* K-12. *Science*
760 *(80-.).* **1997**, *277* (5331), 1453–1462. https://doi.org/10.1126/science.277.5331.1453.

761 (44) Abe, S.; Takayama, K. I.; Kinoshita, S. Taxonomical Studies on Glutamic Acid-Producing Bacteria. *J.*
762 *Gen. Appl. Microbiol.* **1967**, *13* (3). https://doi.org/10.2323/jgam.13.279.

763 (45) Eikmanns, B. J.; Kleinertz, E.; Liehl, W.; Sahm, H. A Family of *Corynebacterium glutamicum*/
764 *Escherichia coli* Expression and Promoter Probing. *Plasmid* **1991**, *102*, 93–98.
765 https://doi.org/10.1016/0378-1119(91)90545-M.

766 (46) Jakoby, M.; Carole-Estelle; Ngouoto-Nkili; Burkovski, A. Construction and Application of New
767 *Corynebacterium glutamicum* Vectors. *Biotechnol. Tech.* **1999**, *13* (6), 437–441.
768 https://doi.org/10.1023/A:1008968419217.

769 (47) Shi, F.; Luan, M.; Li, Y. Ribosomal Binding Site Sequences and Promoters for Expressing Glutamate
770 Decarboxylase and Producing γ-Aminobutyrate in *Corynebacterium glutamicum*. *AMB Express*
771 **2018**, *8* (1). https://doi.org/10.1186/s13568-018-0595-2.

772 (48) Stovicek, V.; Borja, G. M.; Forster, J.; Borodina, I. EasyClone 2.0: Expanded Toolkit of Integrative
773 Vectors for Stable Gene Expression in Industrial *Saccharomyces cerevisiae* Strains. *J. Ind.*
774 *Microbiol. Biotechnol.* **2015**, *42* (11), 1519–1531. https://doi.org/10.1007/s10295-015-1684-8.

775 (49) Van der Rest, M. E.; Lange, C.; Molenaar, D. A Heat Shock Following Electroporation Induces
776 Highly Efficient Transformation of *Corynebacterium glutamicum* with Xenogeneic Plasmid DNA.
777 *Appl. Microbiol. Biotechnol.* **1999**, *52* (4). https://doi.org/10.1007/s002530051557.

778 (50) Cormack, B. P.; Bertram, G.; Egerton, M.; Gow, N. A. R.; Falkow, S.; Brown, A. J. P. Yeast-Enhanced
779 Green Fluorescent Protein (yEGFP): A Reporter of Gene Expression in *Candida albicans*.
780 *Microbiology* **1997**, *143* (2), 303–311. https://doi.org/10.1099/00221287-143-2-303.

781 (51) Nour-Eldin, H. H.; Geu-Flores, F.; Halkier, B. A. USER Cloning and USER Fusion: The Ideal Cloning
782 Techniques for Small and Big Laboratories. In *Plant Secondary Metabolism Engineering*; 2010;
783 Vol. 643, pp 185–200. https://doi.org/10.1007/978-1-60761-723-5.

784 (52) Jensen, N. B.; Strucko, T.; Kildegaard, K. R.; David, F.; Maury, J.; Mortensen, U. H.; Forster, J.;
785 Nielsen, J.; Borodina, I. EasyClone: Method for Iterative Chromosomal Integration of Multiple
786 Genes in *Saccharomyces cerevisiae*. *FEMS Yeast Res.* **2014**, *14* (2), 238–248.
787 https://doi.org/10.1111/1567-1364.12118.

788 (53) Gietz, R. D.; Schiestl, R. H. High-Efficiency Yeast Transformation Using the LiAc/SS Carrier
789 DNA/PEG Method. *Nat. Protoc.* **2007**, *2* (1), 31–34. https://doi.org/10.1038/nprot.2007.13.

790 (54) Mikkelsen, M. D.; Buron, L. D.; Salomonsen, B.; Olsen, C. E.; Hansen, B. G.; Mortensen, U. H.;
791 Halkier, B. A. Microbial Production of Indolylglucosinolate through Engineering of a Multi-Gene
792 Pathway in a Versatile Yeast Expression Platform. *Metab. Eng.* **2012**, *14* (2), 104–111.
793 https://doi.org/10.1016/j.ymben.2012.01.006.

794 (55) Lõoke, M.; Kristjuhan, K.; Kristjuhan, A. Extraction of Genomic DNA from Yeasts for PCR-Based

Applications. *Biotechniques* **2011**, *50* (5), 325–328. https://doi.org/10.2144/000113672.EXTRACTION.

(56) Stirling, D. R.; Swain-Bowden, M. J.; Lucas, A. M.; Carpenter, A. E.; Cimini, B. A.; Goodman, A. CellProfiler 4: Improvements in Speed, Utility and Usability. *BMC Bioinformatics* **2021**, *22* (1). https://doi.org/10.1186/s12859-021-04344-9.

(57) Kamrad, S.; Rodríguez-López, M.; Cotobal, C.; Correia-Melo, C.; Ralser, M.; Bähler, J. Pyphe, a Python Toolbox for Assessing Microbial Growth and Cell Viability in High-Throughput Colony Screens. *Elife* **2020**, *9*. https://doi.org/10.7554/eLife.55160.

(58) Van Rossum, G.; Drake, F. L. *Python 3 Reference Manual*; CreateSpace: Scotts Valley, CA, 2009.

(59) McKinney, W. Data Structures for Statistical Computing in Python. In Proceedings of the 9th Python in Science Conference. In *Proceedings of the 9th Python in Science Conference*; 2010. https://doi.org/10.25080/majora-92bf1922-00a.

(60) Seabold, S.; Perktold, J. Statsmodels: Econometric and Statistical Modeling with Python. In *Proceedings of the 9th Python in Science Conference*; 2010. https://doi.org/10.25080/majora-92bf1922-011.

(61) Bedre, R. Reneshbedre/Bioinfokit: Bioinformatics Data Analysis and Visualization Toolkit. Zenodo 2021. https://doi.org/10.5281/zenodo.4422035.